Available online at www.sciencedirect.com
SCIENCE DIRECT®
Journal of Molecular Catalysis A: Chemical 237 (2005) 1–8
JOURNAL OF MOLECULAR CATALYSIS A: CHEMICAL
www.elsevier.com/locate/molcata

Characterization and reactivity of stannum modified titanium silicalite TS-1 catalysts for transesterification of dimethyl oxalate with phenol

Xinbin Ma [a,*], Jinlong Gong [a,b], Shengping Wang [a], Fei He [a], Hongli Guo [a], Xia Yang [a], Genhui Xu [a]

[a] *Key Laboratory for Green Chemical Technology, School of Chemical Engineering and Technology, Tianjin University, Tianjin 300072, China*
[b] *Department of Chemical Engineering, The University of Texas at Austin, Austin, TX 78712-0231, USA*

Received 21 November 2004; received in revised form 25 April 2005; accepted 26 April 2005
Available online 1 June 2005

Abstract

The transesterification of dimethyl oxalate (DMO) with phenol over stannum modified TS-1 was conducted to prepare methyl phenyl oxalate (MPO) and diphenyl oxalate (DPO), which could be used to produce diphenyl carbonate (DPC). The component, structure and phase of TS-1 catalysts with various Sn loadings were investigated. The relationship between the catalytic properties and the Sn loadings was discussed. The results indicated that, although the Sn-modified TS-1 catalysts had fewer Lewis acid sites than the unmodified TS-1, its catalytic activity was increased greatly by the interaction of Sn with Ti–O–SiO_3 weak Lewis acid centers. The catalyst of TS-1 with 2 wt% Sn loadings performed best, giving 50.3% conversion of dimethyl oxalate and 99.2% selectivity to the target products. By means of X-ray diffraction (XRD), X-ray photoelectron spectroscopy (XPS) and energy dispersive X-ray spectroscopy (EDX), the relationship between the catalytic properties and the structure of Sn dispersed on the surface of TS-1 was studied in detail. At Sn loadings below 2 wt%, Sn was highly dispersed, but at higher loadings it was crystallized into bulk tin dioxide, where the interaction between Ti and Sn was not evidently observed, leading to decreased catalytic activity. XPS results showed that Ti could not be detected even at 1 wt% Sn loadings. EDX results indicated that the content of Ti on the surface decreased with increasing Sn loadings, but the decrease in Ti content was much less than the increase in Sn content. Moreover, NH_3-TPD and FTIR analyses of adsorbed pyridine showed that there were only weak Lewis acid centers on all catalysts and the Sn loadings hardly affected the acid strength of the catalysts.

Keywords: Sn-modified TS-1 catalyst; Transesterification; Diphenyl carbonate; Diphenyl oxalate; Methyl phenyl oxalate; Promotional effect

1. Introduction

Aromatic carbonates have come to occupy an important position as useful organic chemicals for a variety of industrial and synthetic applications. They are used as solvents and as reagents in the transesterification reactions with glycols and bisphenol-A for the production of polycarbonates (PCs) [1].

The industrial methods most commonly employed for the synthesis of aryl carbonates are based on the reaction between a corresponding aromatic alcohol with phosgene in the presence of bases.

Oxidative carbonylation of phenol and transesterification reaction of phenol with dimethyl carbonate (DMC) or dimethyl oxalate (DMO) have been studied to synthesize diphenyl carbonate (DPC) because all these processes [1–10] have avoided using the highly toxic and corrosive phosgene.

Among them, the transesterification of DMO with phenol via a three-step reaction has been deemed as a promising and possible route for DPC synthesis [11,12] from the raw materials such as carbon monoxide, phenol and oxygen. In the first step, dimethyl oxalate is produced by carbonylation of methanol [13]; then, diphenyl oxalate (DPO) is obtained

* Corresponding author. Tel.: +86 22 27406498; fax: +86 22 27890905.
E-mail address: xbma@tju.edu.cn (X. Ma).

1381-1169/$ – see front matter © 2005 Elsevier B.V. All rights reserved.
doi:10.1016/j.molcata.2005.04.052

from transesterification of DMO with phenol; and finally, the decarbonylation of DPO is carried out to produce DPC and carbon monoxide [14], as shown in Eqs. (1)–(3).

$$2CO + 2CH_3OH + 1/2O_2 \rightarrow (COOCH_3)_2 + H_2O \quad (1)$$

$$(COOCH_3)_2 + 2C_6H_5OH \rightarrow (COOC_6H_5)_2 + 2CH_3OH \quad (2)$$

$$(COOC_6H_5)_2 \rightarrow CO(OC_6H_5)_2 + CO \quad (3)$$

The thermodynamic equilibrium constant of reaction (2) at 453 K is estimated at 1.1×10^{-8} [10], from the thermodynamic calculation made with group contribution of liquid components. This indicates that the transesterification between DMO and phenol is not favorable in the thermodynamics. Moreover, the synthesis of diphenyl oxalate follows a two-step reaction module consisting of transesterification of DMO with phenol into methyl phenyl oxalate (MPO) and further disproportionation of MPO into DPO [11,12].

$$(COOCH_3)_2 + C_6H_5OH \rightarrow C_6H_5OOCCOOCH_3 + CH_3OH \quad (4)$$

$$2C_6H_5OOCCOOCH_3 \rightarrow (COOC_6H_5)_2 + (COOCH_3)_2 \quad (5)$$

Nishihira et al. [11,12,14] reported the transesterification of DMO with phenol carried out in the liquid phase using traditional transesterification catalysts such as Lewis acids and soluble organic Pb, Sn, or Ti compounds. In these homogeneous systems, the separation and recovery of the catalysts remains a critical issue when applied to the industrial process. So, the development of active solid catalysts is highly desirable in view of regeneration and separation. Unfortunately, there are few reports on the development of active heterogeneous catalysts for the reaction up to the present time. The goal of our work, therefore, was to develop a heterogeneous catalytic system that combines good catalytic performance with satisfactory recovery of the catalysts used.

Since the discovery of titanium silicate-1 (TS-1) with the MFI structure in 1983 [15], a large number of research projects have been conducted on the synthesis, characterization and catalytic applications of TS-1. TS-1 has unique catalytic properties, being effective in the reaction of a variety of organic compounds at low temperature: epoxidation of alkenes [16–18], epoxidation of olefins [17,19], oxidation of alcohols [20,21], ester exchange [22] hydroxylation, of aromatics [23], and ammoximation of ketones, etc. [18].

More recently, we found that TS-1 can also catalyze the transesterification of phenol with dimethyl oxalate to methyl phenyl oxalate and diphenyl oxalate [24]. The results indicated that the conversion of DMO was not satisfactory although TS-1 showed the excellent selectivity to MPO and DPO. Moreover, there are quite few further studies on the reaction and the characterization of this new catalytic system. Because organic Sn compounds are widely used as ester exchange catalysts [25–28], characterization and activity study stannum modified TS-1 catalyst was performed in this paper for the transesterification of DMO with phenol to find immanent correlation between catalytic performance and catalyst structure.

2. Experimental

2.1. Catalysts preparation

TS-1 (Ti content: 2.5 wt%), obtained from SINOPEC Research Institute of Petroleum Processing, was prepared according to the procedure described in the original patent by Taramasso et al. [15]. It was dried in an oven at 393 K for 2 h to remove the adsorbed water and then calcined in a muffle furnace at 823 K for 4 h in an air atmosphere. This unmodified TS-1 catalyst was stored in a silica gel desiccator prior to use.

To prepare modified TS-1 catalysts with different Sn loadings, the dried TS-1 was impregnated with a toluene solution of dibutyltin dilaurate (as Sn precursor). TS-1 was impregnated with the Sn solutions of different concerntrations to obtain different Sn loadings and the impregnation was performed for 24 h to ensure that the organic Sn compound diffused and dispersed thoroughly on the surface of TS-1. These impregnated samples were dried in an oven for 4 h at 393 K and calcined in a muffle furnace at 873 K for 4 h.

2.2. Characterization techniques

2.2.1. X-ray diffraction (XRD)

X-ray powder diffraction patterns were recorded on a Rigaku C/max-2500 diffractometer using graphite filtered Cu Kα radiation (λ = 1.5405 Å) at 40 kV and 100 mA with a scanning rate of $8^\circ\,min^{-1}$ from $2\theta = 5^\circ$ to $2\theta = 80^\circ$. The XRD phases present in the samples were identified with the help of JCPDS Powder Data Files.

2.2.2. X-ray photoelectron spectroscopy (XPS)

The surface composition and structure of catalyst were studied by X-ray photoelectron spectroscopy (XPS) in a Perkin-Elmer PHI 1600 ESCA system with Mg Kα 1253.6 eV radiation as the excitation source. The samples were mounted on a specimen holder by means of double-sided adhesive tape. Spectra were recorded in steps of 0.15 eV. The C 1s peak (284.5 eV) was used as the internal standard for binding-energy calibration. An estimated error of ±0.1 eV can be assumed for all the measurements. The scanning of the spectra was done at pressures less than 10^{-8} Torr and the temperature was approximately 293 K.

2.2.3. Transmission electron microscopy (TEM)

The samples examined by transmission electron microscopy (TEM) were prepared as follows: The catalysts were

dispersed in ethanol by sonification. Drops of the black suspension were deposited on a holey carbon-coated copper grid, and the ethanol was allowed to evaporate in air. Conventional TEM was carried out on a FEI-Philips Tecai 20 s-twin microscope operated at 100 kV.

2.2.4. Energy dispersive X-ray spectroscopy (EDX)

The chemical composition is determined with a quantitative energy dispersive X-ray analysis EDX (Oxford-6500 instrument installed on a Hitachi H-600 with a 10 nm probe in the range 0–10 keV). The quantification of the spectra was done using CrK- and MoL-lines with ZAF-correction (*Z*: atomic number, which affects the penetration of incident electrons into the material; A: absorption of X-rays in the specimen, on the path to the detector; F: fluorescence caused by other X-rays generated in the specimen).

2.2.5. IR studies

The IR spectroscopic measurements of adsorbed pyridine were carried out on a Bruker Vector22 FTIR spectrometer with 4 cm^{-1} resolution in the 500–4000 cm^{-1} scanning range. The samples were pressed into 10 mg cm^{-2} self-supporting wafers. Prior to each experiment, the catalysts were evacuated (1 Pa) at 693 K for 1.5 h, and then 303 K for 2 h. Following this, the material was exposed to 30 Torr of pyridine for 30 min, and finally evacuated for additional 1 h at 473 K. After adsorption, the samples were out-gassed and the spectra were recorded at room temperature. The treatments were carried out using a quartz IR cell [29].

2.2.6. Temperature programmed desorption of ammonia (NH_3-TPD)

NH_3-TPD experiments were conducted on an Auto-chem 2910 (Micromeritics, USA) instrument. About 100 mg of the oven-dried sample was taken in a U-shaped quartz sample tube and the sample was pretreated in ultra high purity Ar (50 ml min^{-1}) at 393 K for 1 h and then cooled to ambient temperature. The pulses of ammonia were supplied to the samples to saturation. Ammonia was then replaced with argon and the sample was heated to 873 K at a rate of 10 K min^{-1}.

2.3. Catalytic test

The reaction was conducted in a 250 ml glass flask equipped with a thermometer, a distillation apparatus, and a stirrer under refluxing condition at atmosphere pressure. Especially, the top of the distillation column was kept at 353 K by flowing recycled hot water in order to remove methanol from the reaction system. Thus, the reaction equilibrium limitation in reaction (2) was overcome and the reaction was accelerated towards the desired direction. The reaction mixture contained 0.1 mol DMO, 0.5 mol phenol and the catalyst. After the raw materials and the catalyst were placed into the batch reactor, nitrogen gas was flowed at 30 SCCM to purge the air from the reaction system. After 10 min, the nitrogen flow was stopped and the flask was heated at a rate of 8 K min^{-1}. The reaction was conducted at 453 K at an atmospheric pressure. Qualitative and quantitative analyses [30,31] of reaction products and distillates were carried out on HP 5890-HP5971MSD and HP 5890 gas chromatographs equipped with a flame ionization detector. An OV-101packed column was used to separate products for GC analysis. The products were mainly diphenyl oxalate, methyl phenyl oxalate, anisole, and trace amounts of isomer products of anisole. The conversions were reported on the basis of the limiting reagent, DMO, and defined as the ratio of the moles of converted DMO to the moles of DMO fed initially to the reactor. The selectivity to MPO and DPO was defined as the moles of MPO and DPO produced per 100 mol of consumed DMO, and the yields of MPO and DPO were obtained from multiplication of DMO conversion by the selectivity to MPO and DPO.

3. Results and discussion

3.1. Catalytic activity measurements

The transesterification of dimethyl oxalate was carried out at 453 K under atmospheric pressure using stannum modified TS-1. Table 1 demonstrates the variation in conversion level and selectivity to MPO and DPO with Sn loadings range 0 wt%–8 wt%. We reported, in the previous paper [24], that unmodified TS-1 is an active catalyst, giving 26.5% DMO conversion, for the transesterification of DMO with phenol. As shown in Table 1, the conversion of DMO was improved from 26.5% to 50.3%, when the amount of Sn loadings was increased to 2 wt%. It was remarkable that the total selectivity to MPO and DPO still remained about 99%. Interestingly, the selectivity ratio of MPO to DPO was relatively low at this point. As a result, the yield ratio of DPO (15.1%) to MPO (34.9%) showed a maximum at 2 wt% Sn loadings. Thereafter, as Sn above 2 wt% was added, both the conversion of DMO and the yield of MPO and DPO decreased. The previous investigation [28] also indicated that DMO conversion was 31.6% over 2 wt% Sn/SiO_2 catalysts, as against 50.3%

Table 1
The catalytic performance of TS-1 with different Sn loadings[a]

Sn loadings (wt%)	Conversion[b] (%)	Selectivity (%)			Yield (%)	
		AN	MPO	DPO	MPO	DPO
0	26.5	0.8	89.2	10.0	23.6	2.7
1	34.6	1.0	82.3	16.8	28.5	5.8
2	50.3	0.8	69.3	29.9	34.9	15.1
4	28.7	2.7	76.7	20.6	22.0	5.9
8	24.6	2.0	76.7	17.3	19.8	4.0
SnO_2	2.8	7.2	57.1	35.7	1.6	1.0

MPO: methyl phenyl oxalate; DPO: diphenyl oxalate; AN: anisole.
[a] Reaction conditions: catalyst 1.8 g, phenol 0.5 mol; *n*(PhOH)/*n*(DMO) = 5.0; reaction time 2 h, reaction temperature 453 K.
[b] Based on charged DMO.

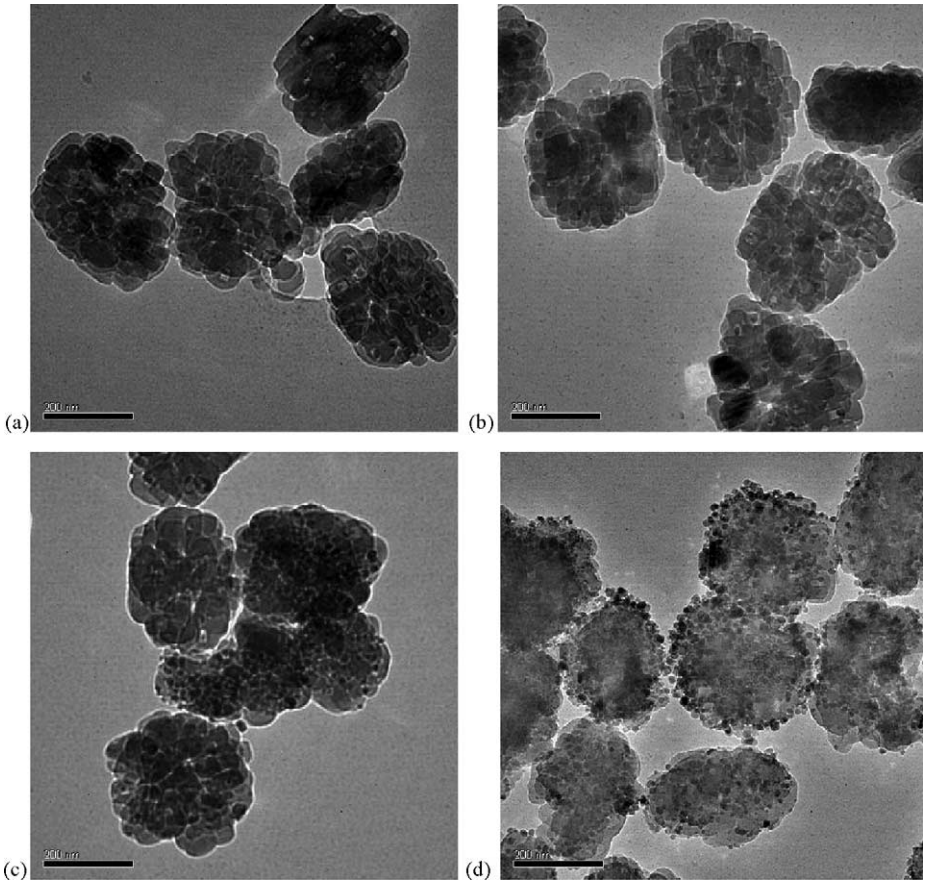

Fig. 1. The TEM photos of TS-1 catalysts with different Sn loadings: (a) 1% Sn; (b) 2% Sn; (c) 4% Sn; (d) 8%Sn.

over 2 wt% Sn/TS-1, which suggested that the interaction between Sn and Ti promoted the catalytic activity of TS-1.

3.2. TEM characterization

This work aims to elucidate the reasons why Sn additive promoted catalytic activity over Sn/TS-1 catalysts. For this purpose, we carried out characterization of catalysts by TEM, X-ray spectroscope (XPS, EDX and XRD) to obtain structural information about Sn species. FT-IR and NH_3-TPD were also conducted in order to observe adsorbed species on catalysts and to follow their behavior.

First, we thought that Sn additive caused some morphological change of TS-1 particles, such as growth of the particle size. So metal particles on the catalysts were directly observed by TEM. Fig. 1 shows the TEM photos of TS-1 catalysts with different Sn loadings.

In the case of 1 wt% and 2 wt% Sn/TS-1, Sn particles were hardly observed and not distributed on the surfaces (Fig. 1(a) (b)), while those on 4 wt% and 8 wt% Sn/TS-1 were omnipresent (Fig. 1(c) and (d)). From Table 1, it was found that the 2 wt% Sn/TS-1 showed the highest DMO conversion and DPO selectivity. But we were not sure whether the difference in appearance of Sn particles caused such a drastic change in reactivity or not. We adopted several other methods of surface characterization to find out the most probable explanation.

3.3. Quantitative analysis by XPS

Surface atomic ratios calculated from XPS peak heights and atomic sensitivities [32] by assuming uniform distribution of all elements, besides carbon, are compared to the nominal atomic composition in order to obtain information on the structure of the surface and the dispersion of the active phases. The simplified formula used for the calculation of relative surface atomic compositions does not take into account inelastic mean free path effects due to the energy difference between the different peaks. The atomic sensitivities obtained from [33] were corrected taking into account the measured energy dependence of our analyzer transmission. In Table 2, the calculated surface atomic ratios and the mass ones, observed for each catalyst sample, are summarized.

In the case of the unmodified TS-1catalyst, it can be noticed that the mass content of Ti are roughly consistent with the one in the bulk phase. This phenomenon was not observed when tin was supported on TS-1. In the meantime, the increase rate of Sn content on surface is close to that of the nominal Sn content within the experimental error. This result indicates that Ti atom on surface has been mantled

Table 2
Surface composition of catalysts with different Sn loadings measured by XPS

Element	0 wt% Sn		1 wt% Sn		2 wt% Sn		4 wt% Sn		8 wt% Sn	
	wt%	at.%	wt%	at.%	wt%	at.%	wt%	at.%	wt%	at.%
O	56.3	69.8	58.5	68.3	57.3	68.8	49.7	68.8	45.7	69.1
Si	41.3	29.2	44.0	31.5	42.7	30.7	36.0	28.5	30.0	25.9
Ti	2.4	1.0	0.0	0.0	0.0	0.0	0.0	0.0	0.0	0.0
Sn	0.0	0.0	1.5	0.2	2.7	0.5	14.3	2.7	24.3	5.0

when the amount of Sn loadings reached 1 wt%. Therefore, the increase in Sn loadings resulted in the formation of crystallized Sn compound. Besides, XPS analysis provided bond energy values equal to 487.4 eV referring to Sn 3d, which is characteristic of Sn(IV). The Sn^{4+} peak of 487.4 eV represented SnO_2 due to dibutyltin dilaurate (DBTDL) as the Sn precursor (Eq. (6)).

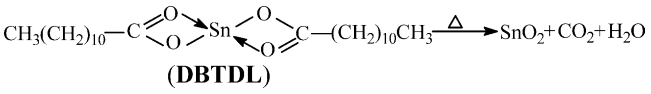

(6)

It has been well established that the XPS intensity ratios of metal cations of the metal oxide to the cations of the support can provide important information regarding the dispersion and crystallite size of supported metal particles [33–35]. The relationship between the Sn 3d/Si 2p ratio and Sn content of the Sn/TS-1 samples is shown in Fig. 2. There are two straight lines with different slopes corresponding respectively to samples with Sn loadings lower and higher than its dispersion capacity, and from the intercept of the two lines we can estimate the dispersed capacity of Sn on TS-1 to be 2.2 wt%.

3.4. XRD analysis

The X-ray powder diffraction analysis was undertaken to determine the composition and crystallinity of Sn species. In the XRD patterns of TS-1 catalysts with or without Sn modification (Fig. 3), the diffraction peaks attributed to the TS-1 were observed on the samples. The XRD analysis showed that there were no characteristic diffraction peaks of Sn species (d = 0.334, 0.264, 0.176 nm) when the loading of Sn was less than 4 wt%. However, when the Sn loadings was increased beyond this borderline, i.e. above its dispersion capacity, the marked change in intensity or offset of peak position can be detected at higher loadings, which indicated that Sn(IV) species was highly dispersed at low Sn loadings and SnO_2 with the tetragonal crystal structure appeared at high loadings. The appearance of SnO_2 phase led to the decrease in the catalytic activity of TS-1. This result was in good agreement with the value obtained from XPS quantitative analysis as well as with that from TEM analysis and catalytic performance.

3.5. EDX characterization

Energy dispersive X-ray spectroscopy (EDX) is an effective method for analyzing the elemental composition of solid surface. Unlike XPS, the analysis depth of EDX for different sample can reach micrometer level. Table 3 exhibits the elemental composition of catalyst surface measured by EDX. As demonstrated, the content of Ti on TS-1 surface was constantly dropped along with the increase in the loaded Sn amount. But, the extent of decreased Ti content is far less

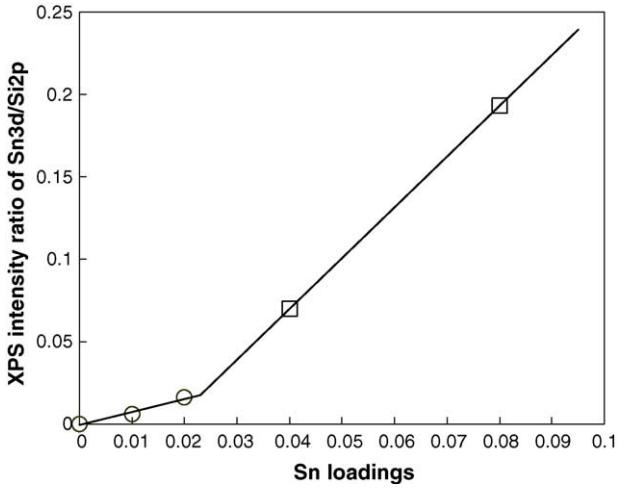

Fig. 2. Correlation between XPS peak intensity ratio of Sn 3d/Si 2p and Sn loadings in the Sn-modified TS-1 samples.

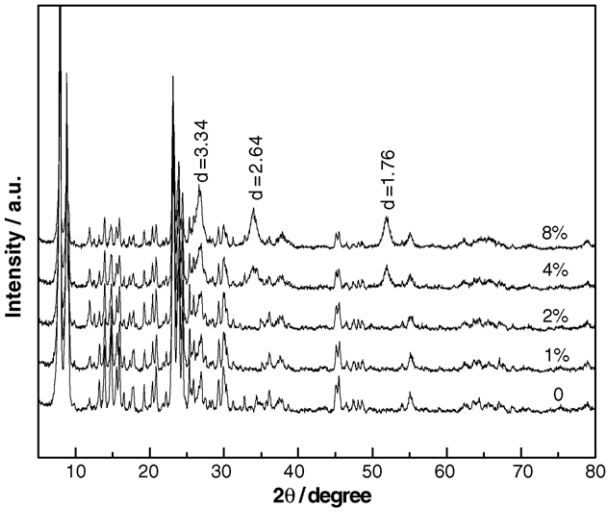

Fig. 3. XRD spectra of TS-1 catalyst with different Sn loadings.

Table 3
Surface composition of catalysts measured by EDX electron energy spectra

Element	1 wt% Sn		2 wt% Sn		4 wt% Sn		8 wt% Sn	
	wt%	at.%	wt%	at.%	wt%	at.%	wt%	at.%
O	56.3	70.4	56.2	70.5	54.0	70.4	52.0	71.4
Si	39.8	28.3	39.3	28.1	36.9	27.4	31.8	26.2
Ti	2.6	1.1	2.5	1.1	2.4	1.0	2.2	1.0
Sn	1.3	0.2	2.0	0.3	6.7	1.2	14.0	2.6

than that of increased Sn. The reason for this case is due to relative increase in Sn loadings. In fact, because EDX can detect bulk phase of sample, the Ti atom determined by EDX is equal to that in bulk phase, especially when loading amount of Sn is low. From Tables 2 and 3, we can see that the Sn content measured by XPS was slightly higher than that measure by EDX at low Sn loadings (2 wt%). However, when Sn loadings increased to 8 wt%, this difference is much clearer. Thus, the results further proved the contrast between depths of information expressed by XPS and EDX.

3.6. Temperature programmed desorption of ammonia analysis

NH_3-TPD characterization was conducted to survey the acid strength of TS-1 catalysts and the influence of Sn loadings on it. In the NH_3-TPD curves, peaks are generally distributed into two regions: below and above 673 K referred to as low-temperature (LT) and high-temperature (HT) regions respectively. The peaks in the HT region can be attributed to the desorption of NH_3 from strong Brönsted and Lewis type acid sites, and the peaks in the LT region are assigned as the desorption of NH_3 from weak acid sites [36,37]. From the result shown in Fig. 4, it can be seen that the peaks appeared only in the low temperature region, confirming that there existed only weak acid sites on the surface of TS-1 catalysts with Sn loadings ranging from 0 wt% to 8 wt%. Furthermore, the maximum temperature offset is 20 K. This indicates that the amount of Sn loadings has little effect on the strength of the surface acid on TS-1. We carried out a preliminary study on the effect of acid strength on the selectivity to anisole and a part of the results was reported elsewhere [24]. Briefly, the weak acid sites are responsible for the formation of MPO, while the strong acid sites were in favor of the formation of anisole. Therefore, the results of TPD gave the reason for high selectivity to MPO and DPO over Sn-modified TS-1 catalysts.

3.7. IR characterization of adsorbed pyridine

FTIR analysis of adsorbed pyridine allows a clear distinction between Brönsted and Lewis acid sites. IR band at 1455 cm^{-1} is attributed to pyridine adsorbed on Lewis acid sites, IR band at 1545 cm^{-1} to that adsorbed on Brönsted acid sites. While the peak at 1490 cm^{-1} can be ascribed to the overlapping of Brönsted acid and Lewis acid sites [38–40]. From Fig. 5, it can be seen that IR pyridine adsorption spectra of TS-1 has peaks at 1455 and 1490 cm^{-1} while the peak at 1545 cm^{-1} is absent. This means that there are only Lewis acid sites, but no Brönsted acid sites on TS-1 whether it is modified with Sn or not. Fig. 6 shows the relative acid amount of TS-1. We found that unmodified TS-1 catalyst had the largest acid amount. From the XPS analysis above, we knew that Ti atom on surface has been mantled when the amount of SnO_2 loadings reached 1 wt%, which reduced the number of the weak Lewis acid center in the Ti–O–SiO_3 structure. So, the relative acid amount of TS-1 dropped from 858 to 560 with increasing Sn loadings from 0 to 1 wt%. Furthermore, the weak acid in SnO_2 rose with the increase in the Sn loadings, which, together with that of weak Lewis acid formed from Ti center, contributed to the gradual, but slow, decrease in relative acid amount.

It is pointed out that the catalytic performance, especially DMO conversion, did not show linear relationship with the

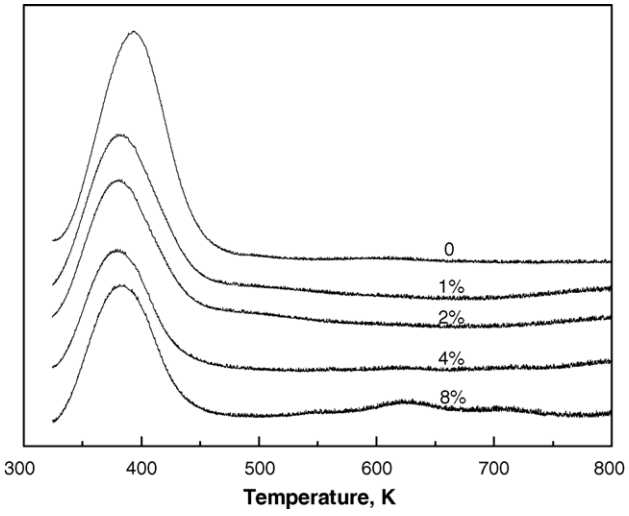

Fig. 4. NH_3-TPD profile of TS-1 catalyst with different Sn loadings.

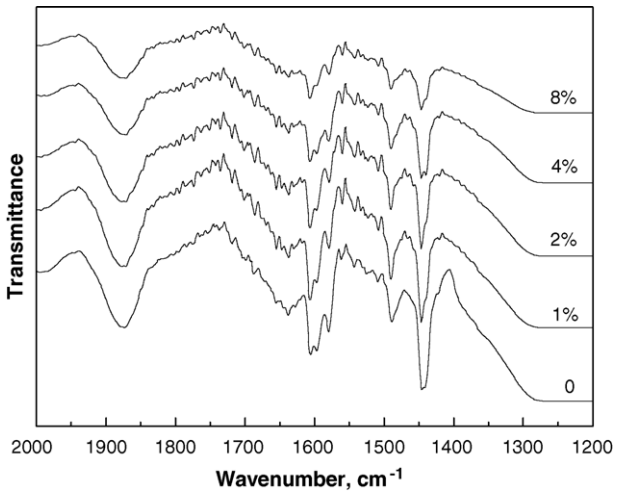

Fig. 5. FTIR spectra absorbed pyridine of TS-1 with different Sn loadings.

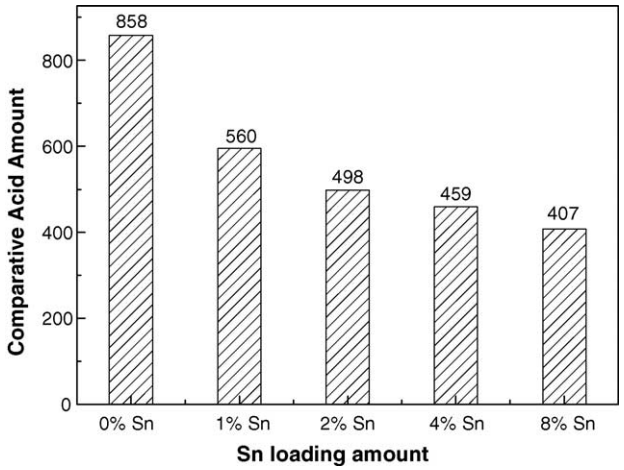

Fig. 6. Relative acid amount of TS-1 with different Sn loadings.

amount of surface acid. The effect of interaction between Sn and Ti–O–SiO_3 offset the decrease in acid amount with increasing Sn loadings, which, as a whole, enhanced the catalytic activity of TS-1. Moreover, Sn active center accelerated the conversion rate of MPO to DPO and enhanced the yield of DPO.

4. Conclusions

The catalytic activities were promoted greatly by the interaction of SnO_2 with Ti–O–SiO_3 weak Lewis acid centers although the Sn-modified TS-1 catalysts had fewer Lewis acid sites than the unmodified TS-1. The catalyst of TS-1 with 2 wt% Sn loadings performed best, giving 50.3% conversion of DMO and 99.2% selectivity to the target products. At Sn loadings below 2 wt%, Sn was highly dispersed, but at high loadings it was crystallized into bulk tin dioxide, and the catalytic activity decreased. XPS results showed that Ti could not be detected even at 1 wt% Sn loadings. The dependence of XPS peak intensity ratio of Sn 3d/Si 2p on the Sn loading estimated the dispersed capacity of Sn on TS-1 to be 2.2 wt%, which was in good agreement with the value obtained from XRD analysis as well as that from TEM analysis and catalytic performance. EDX results indicated that the content of Ti on the surface decreased with increasing Sn loadings, but that the decrease in the Ti content was much less than the increase in the Sn content. NH_3-TPD and FTIR analyses of adsorbed pyridine results showed that there were only weak Lewis acid centers on all catalysts and that the Sn loadings did not have significant effect on the acid strength of the catalysts. The interaction between Sn and Ti–O–SiO_3 played an important role in this reaction system. Sn active centers effectively accelerated the conversion rate of MPO to DPO and potentially promoted the yield of DPO. Further experimental studies that specifically address the structure of Sn-modified TS-1 catalyst are still needed to completely understand these issues.

Acknowledgements

We acknowledge National Natural Science Foundation of China (NSFC) (Grant 20276050) and Tianjin Science and Technology Committee (TSTC) of China (Grant 033103511) for financial support. We also would like to thank two anonymous referees' helpful comments on this work.

References

[1] A.G. Shaikh, S. Sivaram, Chem. Rev. 96 (1996) 951.
[2] Y. Ono, Pure Appl. Chem. 68 (1996) 367.
[3] X.B. Ma, J.L. Gong, X. Yang, S.P. Wang, Appl. Catal. A: Gen. 280 (2005) 215.
[4] W.B. Kim, J.S. Lee, J. Catal. 185 (1999) 307.
[5] K. Okuyama, J. Sugiyama, R. Nagahata, M. Asai, M. Ueda, K. Takeuchi, J. Mol. Catal. A: Chem. 203 (2003) 21.
[6] H. Ishii, M. Goyal, M. Ueda, K. Takeuchi, M. Asai, Appl. Catal. A: Gen. 201 (2000) 101.
[7] J.L. Gong, X.B. Ma, S.P. Wang, J. Mol. Catal. A: Chem. 207 (2004) 215.
[8] X.B. Ma, J.L. Gong, S.P. Wang, J. Mol. Catal. A: Chem. 218 (2004) 253.
[9] X.B. Ma, J.L. Gong, X. Yang, Catal. Commun. 5 (2004) 179.
[10] J.L. Gong, X.B. Ma, X. Yang, S.P. Wang, N. Gao, D.L. Wang, Catal. Lett. 99 (2005) 187.
[11] K. Nishihira, S. Tanaka, K. Harada, R. Sugise, US Patent 5834615 (1997).
[12] K. Nishihira, S. Tanaka, K. Harada, R. Sugise, A. Shiotani, K. Washio, US Patent 5922827 (1999).
[13] T. Matsuzaki, A. Nakamura, Catal. Surv. Jpn. 1 (1997) 77.
[14] K. Nishihira, S. Tanaka, Y. Nishida, I. Hirofumi, S. Fujitsu K. Harada, R. Sugise, US Patent 5811573 (1998).
[15] M. Taramasso, G. Perego, B. Notari, US. Patent 4410501 (1983).
[16] G. Bellussi, A. Carati, M.G. Clerici, G. Maddinelli, R. Millini, J. Catal. 133 (1992) 220.
[17] M.G. Clerici, P. Ingallina, J. Catal. 140 (1993) 71.
[18] B. Notari, Adv. Catal. 41 (1996) 253.
[19] M.G. Clerici, G. Bellussi, U. Romano, J. Catal. 129 (1991) 159.
[20] L.J. Davies, P. McMorn, D. Bethell, P.C.B. Page, J. Mol. Catal. A: Chem. 165 (2001) 243.
[21] M.G. Clerici, Appl. Catal. 68 (1991) 249.
[22] T. Tatsumi, Y. Watanabe, K.A. Koyano, Chem. Commun. (1996) 2281.
[23] A. Thangaraj, R. Kumar, P. Ratnasamy, Appl. Catal. 57 (1990) 1.
[24] X.B. Ma, H.L. Guo, S.P. Wang, Fuel Process Technol. 83 (2003) 275.
[25] I. Gabriello, R. Ugo, T. Renato, Ger. Offen. 2528412. (1976).
[27] I. Masashi, S. Kohei, T. Tatsuro, JP 08188588 (1996).
[26] T. Hideaki, O. Yoshiyuki, M. Atusi, EP 684221 (1995).
[28] S.P. Wang, X.B. Ma, J.L. Gong, Ing. Eng. Chem. Res. 43 (2004) 4027.
[29] J. Foschiera, T. Pizzolato, E. Benvenutti, J. Braz. Chem. Soc. 12 (2001) 159.
[30] S.P. Wang, Z.H. Li, X.B. Ma, G.H. Xu, Chinese J. Anal. Chem. 30 (2002) 829.
[31] S.P. Wang, X.B. Ma, Z.H. Li, G.H. Xu, Chinese J. Anal. Chem. 30 (2002) 1085.
[32] D. Briggs, M.P. Seah (Eds.), Practical Surface Analysis, vol. 1, second ed., Wiley, New York, 1990, p. 201.
[33] Y.C. Xie, Y.Q. Tang, Adv. Catal. 37 (1990) 1.

[34] L. Salvati Jr., L.E. Makovsky, J.M. Stencei, F.R. Brown, D.M. Hercules, J. Phys. Chem. 85 (1981) 3700.
[35] S.C. Fung, J. Catal. 58 (1979) 454.
[36] F. Lónyi, J. Valyon, Microporous Mesoporous Mater. 47 (2001) 293.
[37] M. Sawa, M. Niwa, Y. Murakami, Zeolites 10 (1990) 532.
[38] T. Barzetti, E. Selli, D. Moscotti, L. Forni, J. Chem. Soc., Faraday Trans. 92 (1996) 1401.
[39] T.R. Hughes, H.M. White, J. Phys. Chem. 71 (1967) 2192.
[40] C.A. Emeis, J. Catal. 141 (1993) 347.